Efficient mixing at low Reynolds numbers using polymer additives

Alexander Groisman* & Victor Steinberg*†

* *Department of Physics of Complex Systems, The Weizmann Institute of Science, 76100 Rehovot, Israel*
† *Present address: Department of Applied Physics, Caltech, Pasadena, California 91125, USA*

Mixing in fluids is a rapidly developing area in fluid mechanics[1–3], being an important industrial and environmental problem. The mixing of liquids at low Reynolds numbers is usually quite weak in simple flows, and it requires special devices to be efficient. Recently, the problem of mixing was solved analytically for a simple case of random flow, known as the Batchelor regime[4–8]. Here we demonstrate experimentally that very viscous liquids containing a small amount of high-molecular-weight polymers can be mixed quite efficiently at very low Reynolds numbers, for a simple flow in a curved channel. A polymer concentration of only 0.001% suffices. The presence of the polymers leads to an elastic instability[9] and to irregular flow[10], with velocity spectra corresponding to the Batchelor regime[4–8]. Our detailed observations of the mixing in this regime enable us to confirm several important theoretical predictions: the probability distributions of the concentration exhibit exponential tails[6,8], moments of the distribution decay exponentially along the flow[8], and the spatial correlation function of concentration decays logarithmically.

Solutions of flexible high-molecular-weight polymers are viscoelastic fluids[11]. There are elastic stresses that appear in the polymer solutions in a flow, and that grow nonlinearly with the flow rate[11]. This can lead to many special flow effects, including purely elastic transitions[9,12,13] that qualitatively change the character of the flow at vanishingly small Reynolds numbers, Re. As a result of such transitions secondary vortical flows appear in different systems, where the primary motion is a curvilinear shear flow. The onset of those secondary flows depends on the Weissenberg number, $\mathrm{Wi} = \lambda\dot{\gamma}$, where λ is the polymer relaxation time and $\dot{\gamma}$ is the shear rate. It plays a role analogous to that of Re in competition between nonlinearity and dissipation. As has been reported recently, an elastic flow transition can result in a special kind of turbulent motion, elastic turbulence[10], which arises at arbitrary small Re. In our experiments, we find that irregular flows excited by the elastic stresses in polymer solutions can lead to quite efficient mixing at very low Re.

Our mixing experiments were carried out in a curvilinear channel (Fig. 1a) at room temperature, 22.5 ± 0.5 °C. The total rate of the fluid discharge, Q, was always kept constant, so that the average time of mixing was proportional to the position, N, along the channel (Fig. 1a). We used a solution of 65% saccharose and 1% NaCl in water, with viscosity $\eta_s = 0.153\,\mathrm{Pa\,s}$ and density $\rho = 1.32\,\mathrm{g\,cm^{-3}}$, as a solvent for the polymer. We added polyacrylamide, of $M_w = 1.8 \times 10^7$, at a concentration of 80 p.p.m. by weight. One of the solutions entering the channel (Fig. 1a) also contained an initial concentration, $c_0 = 2$ p.p.m., of a fluorescent dye. The solution viscosity was $\eta = 0.198\,\mathrm{Pa\,s}$ at a shear rate $\dot{\gamma} = 4\,\mathrm{s^{-1}}$. The relaxation time, λ, estimated from the phase shift between the stress and the shear rate in oscillatory tests, was 1.4 s. An estimate for the diffusion coefficient of the dye is given by that for the saccharose molecules, which is about $D = 8.5 \times 10^{-7}\,\mathrm{cm^2\,s^{-1}}$. The characteristic shear rate and the Weissenberg number in the flow are estimated as $\dot{\gamma} = (2Q/d^2)/(d/2) = 4Q/d^3$ and $\mathrm{Wi} = \lambda(4Q/d^3)$, respectively, where d is the channel depth.

The Reynolds number, $\mathrm{Re} = 2Q\rho/(d\eta)$, was always quite small. It reached only 0.6 for the highest Q that we explored. Therefore, flow of the pure solvent remained quite laminar and no mixing occurred; see Fig. 1b. The boundary separating the liquid with and without the dye was smooth and parallel to the direction of the flow, and it only became smeared owing to molecular diffusion as the liquids advanced downstream. The behaviour of the polymer solution was qualitatively different from that of the solvent. The flow was only laminar and stationary up to a value of Q, corresponding to $\mathrm{Wi_c} = 3.2$ (and $\mathrm{Re} = 0.06$), at which point an elastic instability occurred. This instability led to irregular flow and mixing of the

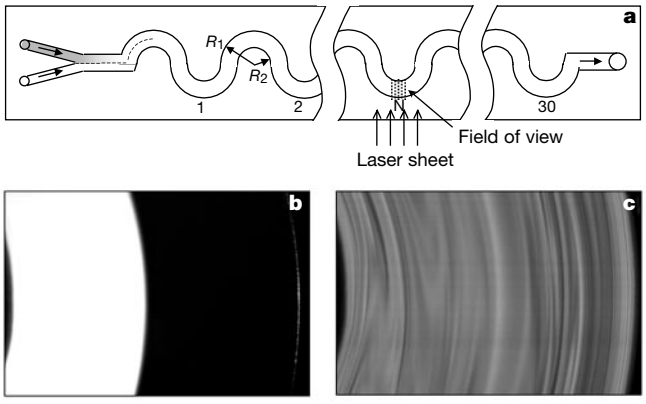

Figure 1 Experimental set-up and two snapshots of the flow. **a**, Experimental set-up. A channel of depth $d = 3$ mm is machined in a transparent bar of perspex and sealed from above by a transparent window. The channel is square in cross-section, and consists of a sequence of 60 smoothly connected half-rings with inner and outer radii $R_1 = 3$ mm and $R_2 = 6$ mm, respectively. The flow is always observed near the middle of a half-ring on the right-hand side of the bar, when viewed downstream. The half-rings on the right-hand side are numbered starting from the channel entrance, and the number, N, of the half-ring is a natural linear coordinate along the channel. Two liquids are fed into the channel by two syringe pumps at equal discharge rates through two separate tubes. The two working liquids are always identical; the only difference is that a small amount of a fluorescent dye (fluorescein) is added to one of them. The channel is illuminated from the side by an argon-ion laser beam converted by two cylindrical lenses to a broad sheet of light, with a thickness of about 40 μm in the region of observation. The fluorescent light emitted by the liquid in the perpendicular direction is projected onto a charge-coupled device (CCD) camera and digitized by an 8-bit, 512 × 512 frame grabber. The concentration of the dye is evaluated from the intensity of the light, which was found to be proportional to the concentration. **b**, **c**, Snapshots of the flow at $N = 29$. Bright regions correspond to high concentrations of the fluorescent dye. Curved boundaries of the channel are seen on the left and on the right. **b**, Pure solvent at $\mathrm{Re} = 0.16$. **c**, Polymer solution at the same flow rate, corresponding to $\mathrm{Wi} = 6.7$.

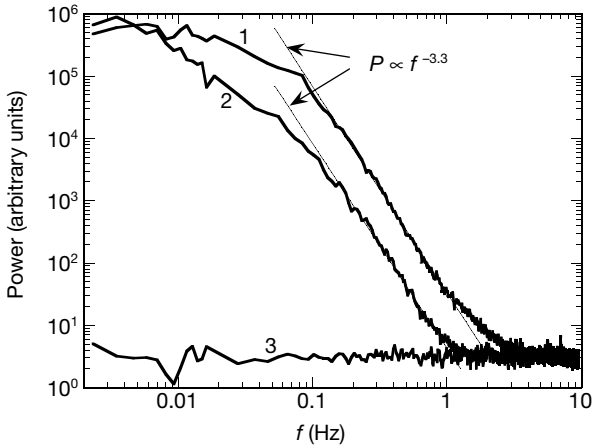

Figure 2 Power, P, of fluctuations of velocity in the middle of the channel at $N = 12$ as a function of frequency, f. The flow velocity was measured by a laser Doppler anemometer, when the region of the laser beam crossing was made very small, $15 \times 15 \times 40\ \mu m$, to decrease the gradient noise. The spectra of the velocity components for the polymer solution are shown: along the mean flow (curve 1), across the mean flow (curve 2) and for the pure solvent across the mean flow (curve 3). The mean velocity for the polymer solution was $\bar{V} = 6.6\ mm\ s^{-1}$. The root mean square, r.m.s., of the fluctuations, $V_{r.m.s.}$, was $0.09\bar{V}$ and $0.04\bar{V}$ in the longitudinal and transverse directions, respectively.

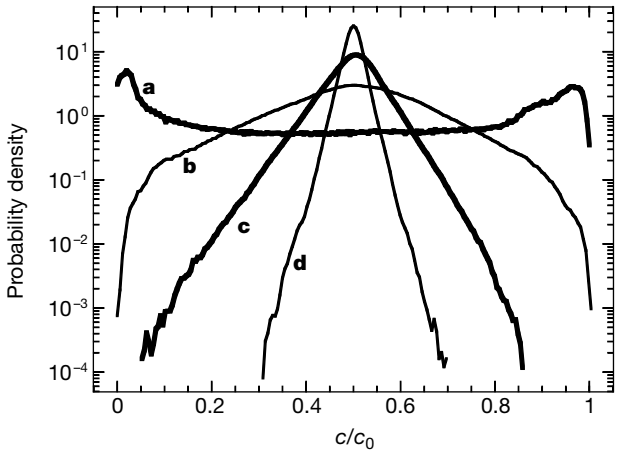

Figure 3 Plots of probability density function (PDF) of the concentration of the fluorescent dye at different positions. The brightness profile was taken 12.5 times per second along a single line across the channel near the middle of a half-ring (a horizontal line in the middle in Fig. 1b and c). Each plot represents statistics over about 10^7 points, corresponding to about 25,000 different moments of time, and a total liquid discharge of $2 \times 10^3 d^3$. The regions near the walls of the channel with widths of $0.1d$ were excluded from the statistics. Curves **a**, **b**: PDF at $N = 8$ and $N = 24$: curves **c**, **d**: with preliminary mixing, at the positions corresponding to $N = 39$ and $N = 54$, respectively.

liquids; see Fig. 1c. The experiments were carried out at Q values of about double the value at the onset of the flow instability, $Wi = 6.7$, where homogeneity of the mixture at the exit of the channel was the highest.

Power spectra of fluctuations of velocity in the centre of the channel at $Wi = 6.7$ are shown in Fig. 2. The spectra of both longitudinal and transversal velocity components do not exhibit any distinct peaks and have broad regions of a power-law decay that is typical for turbulent flow. They resemble the power spectra found at similar Wi values in flow of the same polymer solution between two parallel plates in the regime of elastic turbulence[10]. So, we believe the origin of the irregular flow is the same here as in ref. 10.

According to the Taylor hypothesis fluctuations of the flow velocity in time are mainly due to fluctuations in space advected by the mean flow[2,3]. So the spectra in Fig. 2 imply that the power of the velocity fluctuations scales with the k-number in space as $P \propto k^{-3.3}$. Fluctuations of the velocity gradients should scale then as $k^{-1.3}$, so that the flow becomes increasingly homogeneous at small scales, and mixing is mainly due to the largest eddies, which have the size of the whole system[6]. Such flow conditions correspond to the Batchelor regime of mixing[4,5]. It is one of the two simple cases of random flow, where the problem of mixing has been solved analytically[2,5–8]. The mixing in the irregular flow in the channel gave us an opportunity to study mixing in the Batchelor regime in detail and to test a few important theoretical predictions for the first time, to our knowledge.

Mixing of the polymer solution was a random process. Thus it was appropriate to characterize it statistically, using a probability distribution function (PDF) to find different concentrations, c, of the dye at a point, and the values of the moments, M_i, of the distribution. An ith moment is defined as an average, $\langle |c - \bar{c}|^i \rangle / \bar{c}^i$, where $\bar{c}$ is the average concentration of the dye, which in our case is equal to $c_0/2$. Small values of M_i mean high homogeneity and good mixing of the liquids. The values of M_i are all unity at the channel entrance and become zero for perfectly mixed liquids.

Probability distribution functions of the concentrations at $N = 8$ and $N = 24$ (with $M_1 = 0.72$ and 0.25, respectively) are shown in Fig. 3a and b. Dependencies of M_1 and M_2 on the position N along the channel are presented in Fig. 4. Advanced stages of mixing corresponding to $N > 30$ were studied when the liquids were premixed before they entered the channel (Fig. 4). Representative PDFs in the flow with preliminary mixing taken at the positions where $M_1 = 0.082$ and 0.030 are shown in Fig. 3c and d.

Representative spatial autocorrelation functions for the dye concentration are shown in Fig. 5. At the beginning the concentration distribution is strongly influenced by the initial conditions. There are spatially extended uniform regions with maximal and zero dye concentration, so the concentration remains highly correlated over rather large distances (Fig. 5a) and the PDF has maxima near c_0 and zero (Fig. 3a). As the liquid advances downstream, it becomes increasingly homogeneous. Mixing patterns exhibit many fine-scale structures of different brightnesses (Fig. 1c), the correlation distances become shorter (Fig. 5b) and the PDFs of the dye concentration become narrower (Fig. 3b). The PDF in Fig. 3b has a single peak at $\bar{c}$ and long tails that decay exponentially and touch the limits of the concentration: zero and c_0.

Further downstream, mixing patterns have characteristic features at similar spatial scales (Fig. 5c–e), but are much more faded. The PDF in Fig. 3c is much narrower than in Fig. 3b and has quite clear exponential tails, in agreement with the theoretical predictions[6,7], which implies significant intermittency in mixing[2]. The distribution is well confined in a region far from the limits of zero and c_0. Thus the dependence on the initial conditions should be quite minor by that point. At the last point ($N = 54$, $M_1 = 0.030$) the non-homogeneity in the concentration is hardly seen, and the PDF (Fig. 3d) is very narrow. At an N of about 30 the autocorrelation function reaches some asymptotic form, which does not change as the liquid moves further downstream. This may correspond to the situation when the small-scale structures are smeared by molecular diffusion at the same rate as they are created by the flow. The autocorrelation functions (Fig 5c–e) decay logarithmically at the distances above the diffusion length; this is in agreement with the theoretical predictions for the Batchelor regime[4–6]. The spatial structure of concentration fluctuations in the Batchelor regime has been experimentally studied before in different types of flows[3,14,15]. However, agreement between experiment and theory remained rather controversial (see refs 2, 14 and 15 for discussion).

The dependences of M_1 and M_2 on N in Fig. 4 have inflections at

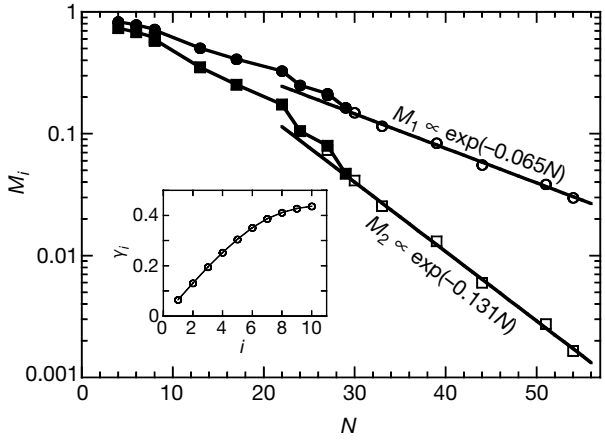

Figure 4 Dependence of M_1 (circles) and M_2 (squares) on the position, N, along the channel. The average flow time is connected to N as $\bar{t} = N \times 7.8$ s. In order to observe stages of mixing corresponding to $N > 30$, we carried out a series of experiments, where the liquids were premixed before they entered the channel. A shorter channel of the same shape was designed for this purpose and put before the entrance to the original one. As a result of this preliminary mixing, the PDF of the dye concentrations at $N = 2$ was almost identical to the PDF at $N = 27$ without the premixing. Filled symbols represent M_1 and M_2 without preliminary mixing. Empty symbols are for the flow with preliminary mixing, when a value of 25 is added to the actual position, in order to match the entrance conditions. We note that these curves are indeed continuations of the dependencies obtained for M_1 and M_2 in the channel without the premixing.

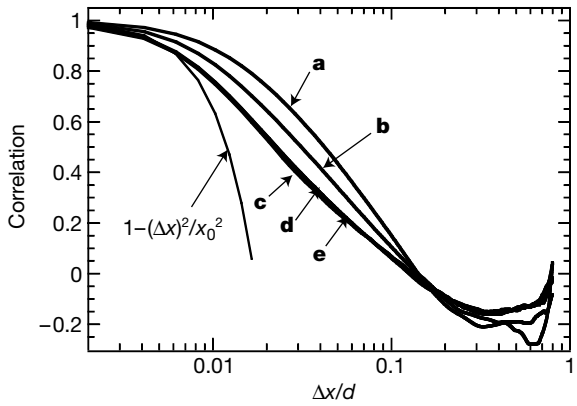

Figure 5 Correlation coefficients for the concentration as functions of the distance Δx across the channel (semilogarithmic coordinates). Curves **a**–**e** correspond to the same conditions as for the PDFs in Fig. 3a–d, and are calculated using the same data arrays. Curve 5 is for $N = 29$. The correlation functions coincide for $N \geqslant 29$. At small Δx they have parabolic scaling with a characteristic length $x_0 = 0.017d \approx 50$ μm. it is probably defined by the thickness of the illuminating light sheet (about 40 μm) and by the molecular diffusion scale, $(D/(V_{r.m.s}/d))^{1/2} \approx 25$ μm. At larger Δx the scaling is logarithmic.

N values between 20 and 30. From the discussion above we suggest that these are due to a transition to an asymptotic regime, where dependence on the initial conditions is lost. The correlation functions at different positions become identical, and PDF of concentrations can be superimposed rather well for Δc of about $3M_1\bar{c}$ around $\bar{c}$ by appropriate stretching of the axes. There is no self-similarity in the shapes of PDF at larger $\Delta c/(M_1\bar{c})$, however, and the shape permanently changes with N. We learn from Fig. 4 that both M_1 and M_2 decay exponentially above $N = 30$, the rate of the decay being twice as high for M_2 as for M_1. In addition, the higher-order moments were found to decay exponentially, $M \propto \exp(-\gamma_i N)$, which is quite in agreement with the theoretical predictions[8]. We note here that M_2, which is the variance of fluctuations of the dye concentration, is often considered as an analogue of the energy of turbulent motion[2]. So its logarithmic derivative, $\mathrm{d}\ln M_2/\mathrm{d}t = -\gamma_2/7.8\ \mathrm{s}^{-1}$ (see Fig. 4), is the analogue of the energy dissipation rate. The theory also predicts linear growth of the coefficients, γ_i, with i at small values and saturation of the growth, when i becomes large[8]. This form of dependence of γ_i on i is quite confirmed by our experimental results; see inset in Fig. 4. The deviation of the dependence of γ_i on i from a straight line at large i values is quantitative evidence for the lack of self-similarity in the mixing. We can see that all our experimental results agree very well with all the theoretical predictions for the Batchelor regime of mixing that we tested[4–8].

As is suggested by the decay of M_1 in Fig. 4, the polymer solutions are mixed at a characteristic distance of $\Delta N \approx 15$. It corresponds to a total path of about $140d$ and an average flow time of about 120 s, which is three orders of magnitude smaller than the diffusion time, d^2/D. Using a more concentrated sugar syrup as a solvent, we prepared a polymer solution with D about 30% smaller and with viscosity and relaxation time about two times larger than those of the original solution. We studied the distribution of c at $N = 29$ in a flow of this solution at the same Wi value of 6.7 as before. Here the characteristic flow velocities were two times lower. Re was about four times lower, and the ratio between the flow time and the diffusion time, d^2/D, was about 1.5 times higher than in the original flow. The measured values of M_1 and M_2 were the same as in Fig. 4, however. Thus the inertial forces and the molecular diffusion did not have any apparent influence on the mixing efficiency. The dependence of the efficiency of mixing at the optimal flow conditions on the concentration of the polymers was surprisingly weak (although Wi_c increased quickly when the polymer concentration was decreasing). So, for a solution with a polymer concentration of 10 p.p.m. ($\eta/\eta_s = 1.03$), M_1 values as low as 0.22 were reached at $N = 29$ (and at $\mathrm{Re} = 0.065$). Mixing was observed down to a polymer concentration of 7 p.p.m. Thus, very viscous liquids can be efficiently mixed in curvilinear channels at very low flow rates with the aid of polymer additives at very low concentrations. This method of mixing, we believe, may find some industrial and laboratory applications. □

Received 17 October 2000; accepted 5 March 2001.

1. Sreenivasan, K. R., Ramshankar, R. & Meneveau, C. Mixing, entrainment, and fractal dimension of interfaces in turbulent flows. *Proc. R. Soc. Lond.* **421,** 79–108 (1989).
2. Shraiman, B. I. & Siggia, E. D. Scalar turbulence. *Nature* **405,** 639–545 (2000).
3. Warhaft, Z. Passive scalars in turbulent flows. *Annu. Rev. Fluid Mech.* **32,** 203–240 (2000).
4. Batchelor, G. K. Small scale variation of convected quantities like temperature in turbulent fluid. *J. Fluid Mech.* **5,** 113–133 (1959).
5. Kraichnan, R. H. Convection of a passive scalar by a quasi-uniform random straining field. *J. Fluid Mech.* **64,** 737–762 (1974).
6. Chertkov, M., Falkovich, G., Kolokolov, I. & Lebedev, V. Statistics of a passive scalar advected by a large scale 2-dimensional velocity field—analytic solution. *Phys. Rev. E* **51,** 5609–5627 (1995).
7. Shraiman, B. I. & Siggia, E. D. Lagrangian path integrals and fluctuations in random flow. *Phys. Rev. E* **49,** 2912–2927 (1994).
8. Balkovsky, E. & Fouxon, A. Universal long-time properties of Lagrangian statistics in the Batchelor regime and their application to the passive scalar problem. *Phys. Rev. E* **60,** 4164–4174 (1999).
9. Larson, R. G., Shaqfeh, E. S. G. & Muller, S. J. A purely viscoelastic instability in Taylor-Couette flow. *J. Fluid Mech.* **218,** 573–600 (1990).
10. Groisman, A. & Steinberg, V. Elastic turbulence in a polymer solution flow. *Nature* **405,** 53–55 (2000).
11. Bird, R. B., Curtiss, C. F., Armstrong, R. C. & Hassager, O. *Dynamics of Polymeric Liquids* (Wiley, New York, 1987).
12. Byars, J. A., Öztekin, A., Brown, R. A. & McKinley, G. H. Spiral instabilities in the flow of highly elastic fluids between rotating parallel disks. *J. Fluid Mech.* **271,** 173–218 (1994).
13. Joo, J. L. & Shaqfeh, E. S. G. Observations of purely elastic instabilities in the Taylor-Dean flow of a Boger fluid. *J. Fluid Mech.* **262,** 27–73 (1994).
14. Miller, P. L. & Dimotakis, P. E. Measurements of scalar power spectra in high Schmidt number turbulent jets. *J. Fluid Mech.* **308,** 129–146 (1996).
15. Williams, B. S., Marteau, D. & Gollub, J. P. Mixing of a passive scalar in magnetically forced two-dimensional turbulence. *Phys. Fluids* **9,** 2061–2080 (1997).

Acknowledgements

We thank G. Falkovich for theoretical guidance and discussions. The work was partially supported by the Minerva Center for Nonlinear Physics of Complex Systems, by a Research Grant from the Henry Gutwirth Fund and by an Israel Science Foundation grant.

Correspondence and requests for materials should be addressed to V.S. (e-mail: victor.steinberg@weizmann.ac.il).

Magnetic-field-induced superconductivity in a two-dimensional organic conductor

S. Uji*, H. Shinagawa*, T. Terashima*, T. Yakabe*, Y. Terai*, M. Tokumoto†, A. Kobayashi‡, H. Tanaka§ & H. Kobayashi§

** National Research Institute for Metals, Tsukuba, Ibaraki 305-0003, Japan*
† Electrotechnical laboratory, Tsukuba, Ibaraki 305-8568, Japan
‡ Research Centre for Spectrochemistry, Graduate School of Science, The University of Tokyo, Bunkyo-ku, Tokyo 113-0033, Japan
§ Institute for Molecular Science, Okazaki, Aichi 444-8585, Japan

The application of a sufficiently strong magnetic field to a superconductor will, in general, destroy the superconducting state. Two mechanisms are responsible for this. The first is the Zeeman effect[1,2], which breaks apart the paired electrons if they are in a spin-singlet (but not a spin-triplet) state. The second is the so-called 'orbital' effect, whereby the vortices penetrate into the superconductors and the energy gain due to the formation of the paired electrons is lost[3]. For the case of layered, two-dimensional superconductors, such as the high-T_c copper oxides, the orbital effect is reduced when the applied magnetic field is parallel to the conducting layers[4]. Here we report resistance and magnetic-torque experiments on single crystals of the quasi-two-dimensional organic conductor λ-$(BETS)_2FeCl_4$, where BETS is bis(ethylenedithio)tetraselenafulvalene[5–8]. We find that for magnetic fields applied exactly parallel to the conducting layers of the crystals, superconductivity is induced for fields above 17 T at a temperature of 0.1 K. The resulting phase diagram indicates that the transition temperature increases with magnetic field, that is, the superconducting state is further stabilized with magnetic field.

Studies on organic conductors have brought us deep understanding of physics in low-dimensional electronic systems. Members of the BETS family containing magnetic Fe ions among various organic conductors have been extensively studied over the past ten years because strong competition is expected between the antiferromagnetic order of the Fe moments and the superconductivity[5,6]. Of these, λ-$(BETS)_2FeCl_4$ has an unusual phase diagram, shown in Fig. 1a. At zero magnetic field, λ-$(BETS)_2FeCl_4$ shows a metal–insulator transition at 8 K (ref. 5), whereas the iso-structural salt λ-$(BETS)_2GaCl_4$ undergoes a superconducting transition around 6 K (ref. 7). The metal–insulator transition is associated with the antiferromagnetic order of the Fe moments[5,8]. The ordered Fe moments are canted by a magnetic field of about 1 T, but the electronic state remains insulating. The insulating phase is destabilized by magnetic fields above about 10 T, and a paramagnetic metallic state is then recovered.

λ-$(BETS)_2FeCl_4$ has a triclinic unit cell[6]. The planar BETS molecules are stacked along the *a* and *c* axes, and consequently form two-dimensional conduction layers (Fig. 1b). The $FeCl_4$ ion (insulating) layer is intercalated between the BETS layers, which makes the *b* axis the least conducting direction. Because of the short interatomic distance between the BETS and $FeCl_4$, finite interactions between the π (conduction) electron on the BETS molecules and the Fe^{3+} 3*d* electrons are expected. The band calculation predicts that λ-$(BETS)_2FeCl_4$ has one closed (two-dimensional) and two open Fermi surfaces in the metallic phase as shown in Fig. 1c (refs 5, 6).

The needle-like single crystals of λ-$(BETS)_2FeCl_4$, elongating along the *c* axis, were prepared by electrochemical oxidation in an appropriate solvent[6]. The resistance was measured by a conventional four-probe a.c. technique with electric current along the b^* axis, which is perpendicular to the *a*–*c* plane. Four gold wires (of diameter 10 μm) were attached to the sample by gold or carbon paint. The magnetic torque was measured by a simple cantilever technique[7]. The experiments were made with a dilution refrigerator and a 20-T superconducting magnet.

The interlayer resistance with a current *t* parallel to the b^* axis ($I_{\|b^*}$) for a magnetic field *B* parallel to the *c* axis ($B_{\|c}$) is presented in Fig. 2a. The insulator–metal transition takes place at around 10.5 T. At 0.04 K, the resistance increases with increasing field after the insulator–metal transition, has a broad maximum around 14 T, and then suddenly decreases by three orders of magnitude. Above 18 T, the detected sample voltage becomes smaller than the noise level, which suggests a superconducting phase transition. As temperature

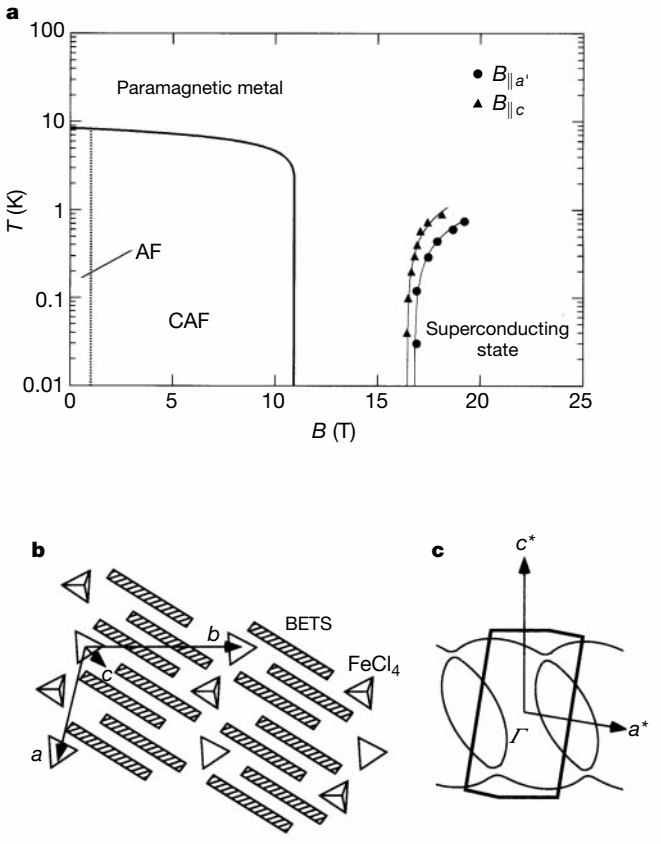

Figure 1 a, Temperature versus magnetic field phase diagram for λ-$(BETS)_2FeCl_4$ when the magnetic field is applied parallel to the *a*′ or *c* axis. At zero magnetic field, a metal–insulator transition takes place at around 8 K. In the insulating phase, the Fe moments are antiferromagnetically ordered. AF and CAF indicate the antiferromagnetic and canted antiferromagnetic phases, respectively. The superconducting phase is induced above 17 T. **b**, Schematic picture of the crystal structure of λ-$(BETS)_2FeCl_4$. The *a*–*c* plane is the conduction layer and the b axis is the least conducting axis. **c**, Calculated Fermi surfaces in the k_a–k_c plane. The area surrounded by thick lines shows the first Brillouin zone. There are one closed (two-dimensional) and two open Fermi surfaces.